Materials Science and Engineering B 311 (2025) 117838

Contents lists available at ScienceDirect

Materials Science & Engineering B

journal homepage: www.elsevier.com/locate/mseb

Cobalt iron oxide ($CoFe_2O_4$) reinforced polyvinyl alcohol (PVA) based magnetoactive polymer nanocomposites for remote actuation

Ans Al Rashid [a,*], Noor A. Al-Maslamani [b], Anas Abutaha [c], Mokarram Hossain [d], Muammer Koç [a]

[a] Division of Sustainable Development, College of Science and Engineering, Hamad Bin Khalifa University, Qatar Foundation, Doha 34110, Qatar
[b] Qatar Biomedical Research Institute, Hamad Bin Khalifa University, Qatar Foundation, Doha 34110, Qatar
[c] Qatar Environment and Energy Research Institute (QEERI), Hamad Bin Khalifa University, Qatar Foundation, Doha 34110, Qatar
[d] Zienkiewicz Institute for Modelling, Data and AI, Faculty of Science and Engineering, Swansea University, Swansea SA1 8EN, United Kingdom

ARTICLE INFO

Keywords:
Magnetoactive polymer composites
Smart materials
Magnetic properties
Biocompatibility
Remote actuation

ABSTRACT

Magnetoactive polymer composites (MAPCs) are materials composed of a polymer matrix embedded with magnetic particles that mechanically respond to external magnetic fields. MAPCs can be programmed to be adjusted remotely without physical interventions using a magnetic field to generate the desired response; therefore, MAPCs are being actively explored for their applications in remote sensing, soft robotics, electronics, and biomedical areas. In this work, novel MAPCs were synthesised comprising polyvinyl alcohol (PVA) as the matrix and cobalt iron oxide ($CoFe_2O_4$) nanoparticles as the magnetic component with varying concentrations (i.e., 1.25%, 2.5%, and 5%). MAPCs were synthesised using the solution casting technique, and field emission scanning electron microscopy (FE-SEM) and x-ray diffraction (XRD) results revealed the successful integration of $CoFe_2O_4$ nanoparticles within the polymer matrix. The synthesised MAPC films were also characterised for their chemical, thermal, magnetic, and biological properties. The incorporation of $CoFe_2O_4$ nanoparticles resulted in an improved magnetic response, with improvements in these properties with increasing $CoFe_2O_4$ content. PVA/5% $CoFe_2O_4$ revealed toxicity and requires further investigation of using these materials with higher $CoFe_2O_4$ concentrations. The magnetic response and biological properties of the PVA/$CoFe_2O_4$ MAPCs revealed their potential uses for remote actuation and sensing in the biomedical sector.

1. Introduction

Magnetoactive polymer composites (MAPCs) are an emerging class of smart materials, pushing the boundaries of material science, comprising a polymer matrix incorporating magnetic-sensitive micron to nanoscale particles [1]. MAPCs combine the adaptability and flexibility of polymers with the responsiveness of magnetic particles, allowing them to transform their shape or properties in the presence of an external magnetic field [2,3]. MAPCs are classified into magneto-strictive and magneto-rheological polymer composites. Magneto-strictive composites deform under a magnetic field, bending or twisting the material [4,5], while magneto-rheological composites contain dispersed magnetic particles that align under a magnetic field, altering the composite's stiffness or rheology [6–8]. Unlike magneto-rheological elastomers (MREs), which use elastomeric polymers, magnetoactive hydrogels replace the polymer matrix with a water-based hydrogel [9–11]. MAPCs can also be categorized as anisotropic or isotropic based on the alignment of magnetic particles within the matrix [12]. MAPCs respond to an external magnetic field to generate controllable and tunable magneto-mechanical responses [13]; therefore, they are widely explored for applications in aerospace, civil, robotics, remote sensing and biomedical sectors, to mention a few [14–19]. The development and utilisation of MAPCs in functional applications require multi-faced optimisation regarding material composition, stimuli response and application-specific testing and characterisation.

Several studies investigated the impact of different materials and their compositions on the magnetic response of MAPCs. Zhang et al. [20] synthesised poly-dimethyl siloxane (PDMS) based MREs using carbonyl iron powder (CIP) in which off-axis anisotropic MREs were produced by a varying orientation of magnetic field during the vulcanisation process. The MREs with larger orientation angles (i.e., 15°) revealed a higher shear modulus with and without an external magnetic field. The increased shear modulus is directly related to the increased magnetic flux density. They also demonstrated the magneto-deformation

* Corresponding authors.
E-mail addresses: aalrashid@hbku.edu.qa, ans.ravian@gmail.com (A. Al Rashid), mkoc@hbku.edu.qa (M. Koç).

https://doi.org/10.1016/j.mseb.2024.117838
Received 11 August 2024; Received in revised form 27 October 2024; Accepted 11 November 2024
Available online 16 November 2024

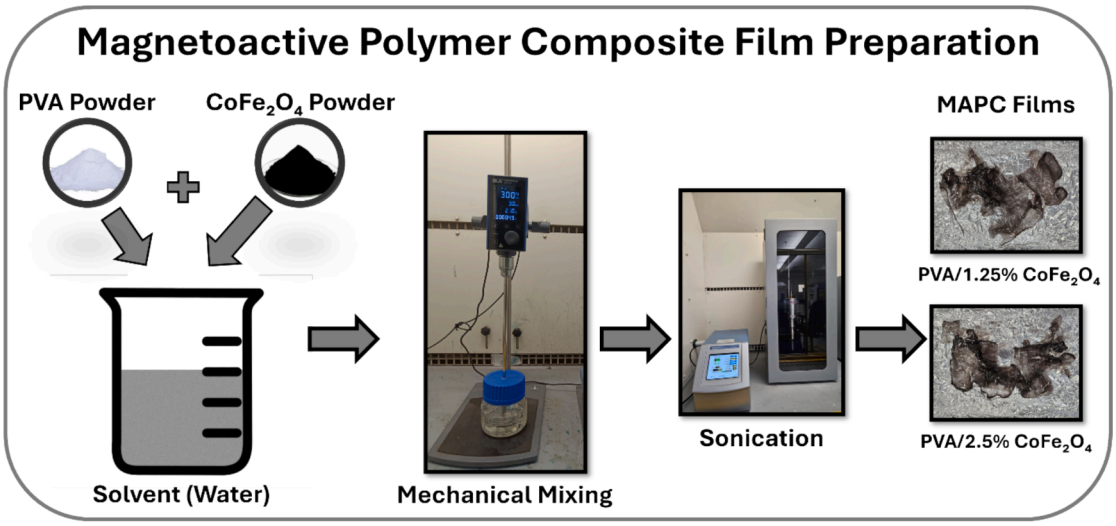

Fig. 1. Magnetoactive polymer composite (MAPC) film synthesis, where PVA and $CoFe_2O_4$ powders were mixed in the solvent (water) using mechanical mixing and ultrasonication techniques. The solution was cast on a flat surface and left at room temperature for 48 h to produce MAPC films.

behaviour of off-axis anisotropic MRE composites. Similar to synthesising MAPCs using elastomeric matrices, Vazquez-Perez et al. [21] created magnetic hydrogels by combining a hydrogel (base) filled with magnetic particle clusters. When exposed to a magnetic field, these magnetic hydrogels significantly stretched and returned to their original shape upon removal of the applied field. The amount of magnetic field-induced stretch depends on the hydrogel stiffness, magnetic particle concentration, and how the particles are distributed within the hydrogel. Soft materials with field-dependent stiffness open new doors for applications such as magnetically controlled valves. Garcia-Gonzalez et al. [22] developed soft elastomeric-based self-healing MAPCs containing NdFeB magnetic nanoparticles and CIPs. The resulting MAPCs could sustain loads beyond 20% strain after several fracture cycles without compromising the structural integrity under tensile loading conditions. It was also observed that the self-healed materials did not experience mechanical degradation and withstood higher stresses than the original material. Takahashi et al. [23] studied the influence of coating iron (CI) particles in a rubbery MRE with a thin layer of plastic (PMMA), which affects its stiffness under an external magnetic field. The PMMA coating reduced the stiffening effect and increased the apparent particle size (from 6.7 μm to 8.4 μm) due to clumping observed in microscopic images, suggesting PMMA-coated particles may not be ideal for MREs designed to stiffen under magnetic fields.

Moreover, the literature also reports the application-specific exploration of MAPCs [24,25]. For instance, Breger et al. [26] fabricated microgrippers using photopatterned hydrogels poly(N-isopropylacrylamide-co-acrylic acid) (pNIPAM-AAc) to achieve self-folding due to swelling response. Gripping ability and remote actuation were achieved by incorporating stiff, non-swellable polypropylene fumarate (PPF) polymer and iron oxide (Fe_2O_3) nanoparticles, respectively. These hydrogel-based grippers with tunable properties hold promise for soft robotic and surgical applications. Likewise, Vasilyeva et al. [27] studied elastomers filled with coarse magnetic particles (60 %) for use in a magnetic pump. Such elastomers exhibited increased strength (38 %) and elasticity (30 %) when exposed to a magnetic field, alone or combined with heat. Chen et al. [28] studied vibration response by adding nonmagnetic particles to MREs made from magnetic and nonmagnetic materials (e.g., iron oxide and rubber). They revealed that bimodal MREs (5 mm and 10 mm thick) significantly increased natural frequency (up to 224 Hz) under a magnetic field compared to regular MREs, which suggests potential tunable vibration control using MRE-based vibration dampers. Borin et al. [29] developed an MRE filled with a nickel–iron alloy (permalloy) instead of typical iron particles, which exhibited significant stiffening (200x increase in the shear modulus) under a moderate magnetic field (400 mT). They proposed that chains formed by the alloy particles within the elastomer are critical to such a stiffening effect, which can be used with controllable stiffness for applications like magnetic dampers. Kolesnikova et al. [30] investigated a soft, magnetic material filled with magnetic and electric microparticles for soft robotics applications. The study focused on exploring the effect of electric particles on the magnetism of the material.

Bastola and Hossain [31] investigated core–shell MREs [32] using rubbery materials filled with magnetic particles. The addition of smaller magnetic nanoparticles within these core–shell structures was explored to improve the MRE's response under a magnetic field. The results revealed that nanoparticles enhanced the overall rheological properties, including reducing the settling of the magnetic particles and significantly improving the stiffening effect when exposed to a magnetic field. Likewise, Kim et al. [33] created a new soft composite combining a magneto-rheological fluid (MRF) and an MRE that can stiffen when exposed to a magnet. This magnetically controlled stiffness (up to 300 % change) makes it a promising material for wearable and foldable devices where local flexibility control is desired. Bastola et al. [34] also created a new type of MRE using 3D printing, which incorporated magnetic fluid pockets within a rubber matrix, allowing for layer-by-layer control of the material's structure. Like traditional MREs, the 3D-printed version stiffened and absorbed vibrations more under a magnetic field, with a more prominent damping effect.

Furthermore, there has been some interest in developing numerical modelling approaches to predict the response of MAPCs under external magnetic fields [35–38]. Romeis and Saphiannikova [39] proposed a new method to model the magnetic behaviour of composite materials. Instead of complex calculations for each tiny particle, this method treats the material as a whole while considering the properties and arrangement of its different parts. This approach allows for the efficient modelling of various composite materials, including those with linear and saturated magnetisation behaviours and isotropic or anisotropic particle arrangements. The method requires minimal computation compared to traditional approaches and can be directly applied to model the magnetic behaviour of composite materials with specific shapes.

It is evident from the literature review that there is an eminent need to develop novel MAPCs for remote actuation and sensing applications in biomedical engineering [40]. Polyvinyl alcohol (PVA) and cobalt iron oxide ($CoFe_2O_4$) are two increasingly essential materials in biomedicine due to their unique properties such as biocompatibility, biodegradability that offer excellent potentials for drug delivery, tissue engineering

Table 1
Compositions of synthesised PVA/$CoFe_2O_4$ MAPCs.

Materials	PVA (wt %)	$CoFe_2O_4$ (wt %)
PVA	100	0
PVA/1.25 % $CoFe_2O_4$	98.75	1.25
PVA/2.5 % $CoFe_2O_4$	97.5	2.5
PVA/5% $CoFe_2O_4$	95	5

scaffolds, and biosensors. Their tailorable properties allow researchers to design materials and devices that can be used as adhesives, textiles, food packaging, construction and biomedical [41–45]. Ferrites, such as $CoFe_2O_4$, with their superparamagnetic properties, are being explored for use in magnetic resonance imaging (MRI) contrast agents and targeted drug delivery due to their ability to be manipulated by external magnetic fields [46–48]. Few studies in the literature attempted to produce PVA/$CoFe_2O_4$ composites to understand their physiochemical and mechanical properties [49,50]. However, to the best of the authors' knowledge, no study in the literature explores using PVA and $CoFe_2O_4$ nanoparticles to synthesise MAPCs for remote actuation and sensing with a specific focus on their potential biomedical applications. The synthesised MAPCs in this study were characterised for their microscopic, chemical, thermal, magnetic, and biological properties. Magnetic response and biological properties of the PVA/$CoFe_2O_4$ nanocomposites revealed that they could be potential candidates for remote actuation and sensing applications in the biomedical sector.

2. Materials and Methods

2.1. Materials

Polyvinyl alcohol (PVA) powder with molecular weight (M_w ~ 89,000–98,000) was procured from Sigma Aldrich (United States), with a melting point of 250℃ and density 1.19–1.31 g/cm^3, as per manufacturer safety data sheet (SDS). Cobalt iron oxide ($CoFe_2O_4$) nanoparticles with an average particle size of 30 nm and purity of 99% were also purchased from Sigma Aldrich. The raw materials were used as received without any pre-processing or purification.

2.2. PVA/$CoFe_2O_4$ nanocomposites synthesis

PVA/$CoFe_2O_4$ MAPCs films were synthesised using a solution casting technique (as demonstrated in Fig. 1), as it is widely reported as an effective approach to achieve stabilised and homogenous particle-reinforced polymer composites [51]. First, 10 g of PVA powder was mixed in 100 ml of deionised water using a mechanical stirrer for 10 min, followed by an ultrasonication (using Qsonica Q700 Sonicator, United States) process for another 10 min, resulting in complete dissolution of PVA within the water. Subsequently, $CoFe_2O_4$ nanoparticles were added to the clear PVA solution during mechanical stirring. The solution was then subjected to an ultrasonication process for 10 min to ensure the homogenous dispersion of $CoFe_2O_4$ nanoparticles within the PVA solution. Three different PVA/$CoFe_2O_4$ MAPCs compositions were prepared by varying the weight per cent of the nanoparticles within the PVA matrix, i.e., 1.25%, 2.5%, and 5% (as detailed in Table 1). The resulting PVA/$CoFe_2O_4$ solutions were cast on flat surfaces and left at room temperature for 48 h to produce MAPC films (1 mm thickness) and to remove the excess water content. A similar procedure was adopted in the literature for solvent removal from polymer composite films [52–54].

2.3. Characterisation

Scanning electron microscopy (SEM) provides insights into the surface morphology of composites, revealing nanoparticle dispersion and potential interactions with polymers, while energy dispersive X-ray spectrometer (EDS) identifies the elements present within the composites, verifying nanoparticle composition and highlighting any impurities. The morphology of MAPCs films was observed under a field emission scanning electron microscopy (FE-SEM, FEI Quanta650FEG) at an acceleration voltage of 20 kV and a working distance of 0.9 cm, equipped with EDS. The prepared MAPCs were characterized by X-ray diffraction (XRD) using the Rigaku SmartLab system with Bragg-Brentano (2θ-θ) geometry. All composite sheets were cut into 1 cm × 1 cm pieces and were placed horizontally on the sample holder. Before the XRD scans, the samples were aligned properly at the half of the X-ray beam and positioned at the same axis of the source and the detector when 2θ and θ were at zero. XRD scans of 2θ-θ were then acquired in the range of 3-90° with a step size of 0.02° for 1.5 h per sample.

Fourier transform infrared (FTIR) analyses the chemical bonds in the composite, revealing interactions between polymer and nanoparticles and the presence of functional groups for desired functionalities. FTIR analysis was performed using a Nicolet iS50 FT-IR spectrometer (Thermo Scientific, United States) with an attenuated total reflectance (ATR) sampling accessory featuring a diamond crystal plate to determine the molecular structure of the synthesised MAPCs. The FTIR analysis was performed with 32 scans/sample in the spectral range between 500 cm^{-1} and 4000 cm^{-1} at a high spectral resolution (4 cm^{-1}). Thermogravimetric analysis (TGA) measures the weight change of the composite under increasing temperature, providing insights into thermal stability and degradation behaviour. TGA analysis was performed using a Thermal Analyzer (SDT 650, TA Instruments, United States) under a nitrogen environment, where the MAPCs were placed within a ceramic crucible carefully and subjected to heating from 50℃ to 650℃ at a rate of 10℃/min.

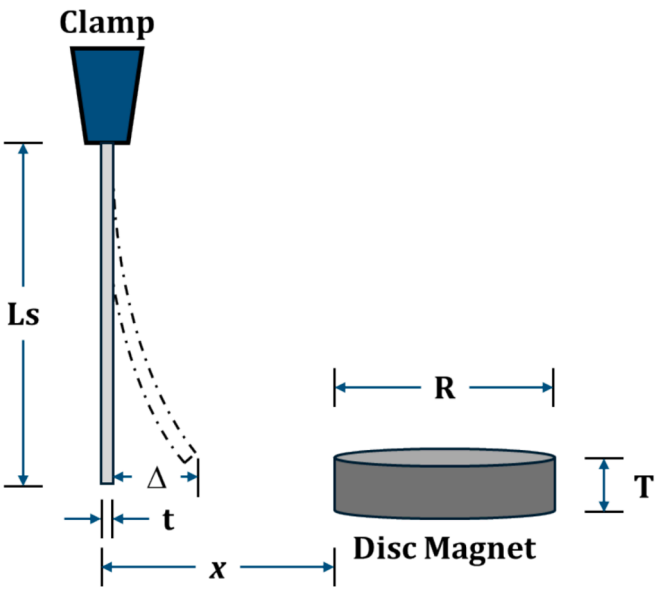

Fig. 2. Schematic diagram of the experimental setup for magnetic actuation response. The magnetoactive polymer composite (MAPC) strips were clamped at one end, a permanent magnet was placed at different distances from the sample (corresponding to variable magnetic field intensities), and MAPC strip deflection at the tip was recorded.

2.4. Magnetic properties and actuation response

Magnetic properties of the base materials and MAPCs were examined using a vibrating sample magnetometer (Quantum Design Dynacool PPMS) under the magnetic fields from 0 kOe to 10kOe at ambient temperature. Hysteresis loops were recorded for all the materials to obtain saturation magnetisation (M_s), coercivity (H_c), and remanence (M_r). The actuation response of PVA/$CoFe_2O_4$ MAPCs was investigated

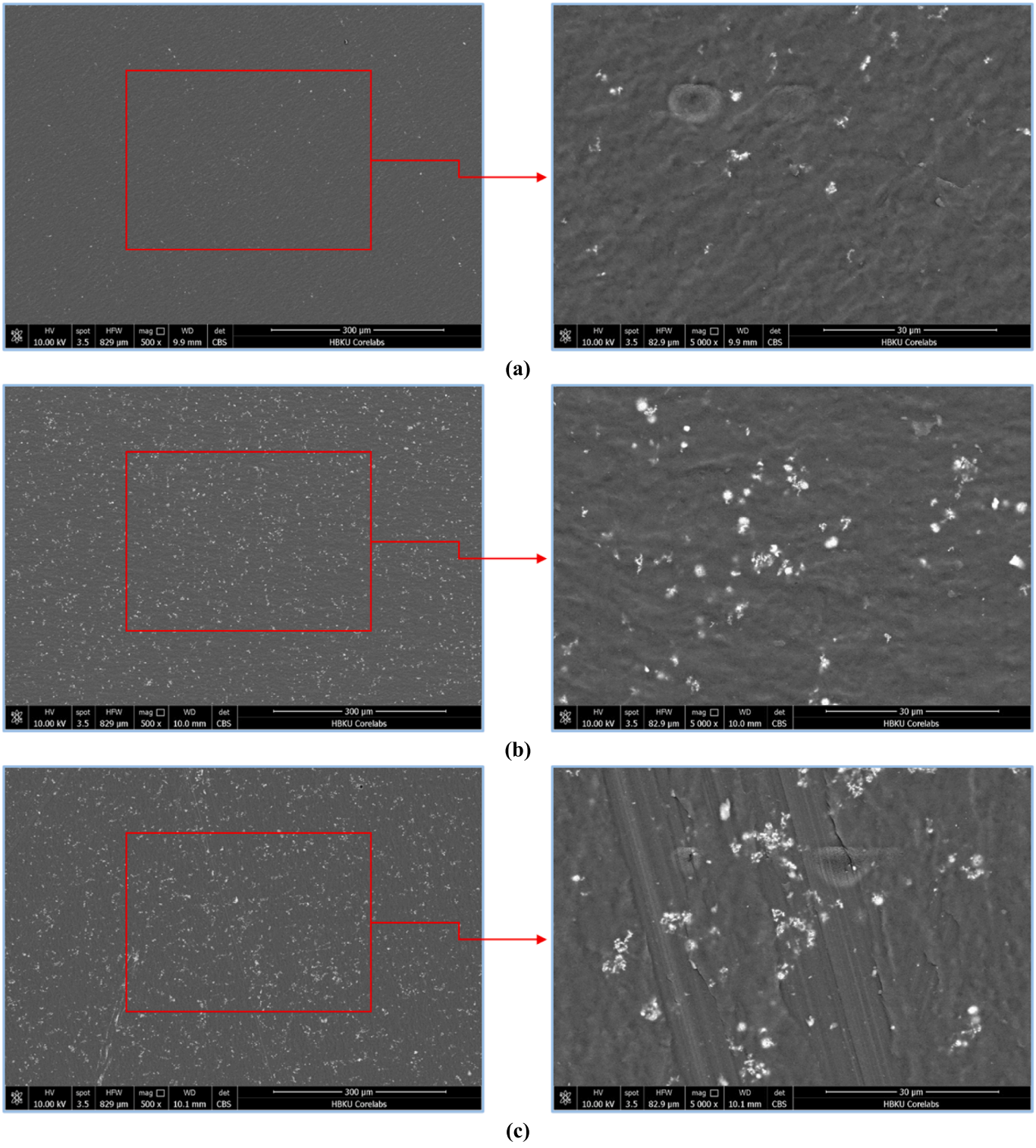

Fig. 3. Scanning electron microscopy (SEM) analysis for different magnetoactive polymer composite (MAPC) films synthesised **(a)** PVA/1.25% $CoFe_2O_4$ **(b)** PVA/2.5% $CoFe_2O_4$ **(c)** PVA/5% $CoFe_2O_4$. The images on the left are captured at 500x magnification and those on the right at higher magnification levels (5000x), presenting the homogenous dispersion of $CoFe_2O_4$ nanoparticle. However, some agglomeration was observed at higher concentrations (i.e., PVA/5% $CoFe_2O_4$).

using mould-casted specimens (measuring 50 mm × 12 mm × 0.2 mm). An external magnetic stimulus was applied to the MAPC strips clamped at one end, as reported in Fig. 2. A magnetic flux density was varied between 0 and 2900G by adjusting the distance between the free end of the MAPC strips and the permanent disc magnet (N42 Neodymium Disc Magnet, with flux density (B_r) of 13,050 G, 2 in diameter and 1 in thickness). The magnetic field (B_x) at a distance (x) from the magnet was calculated using the following equation (1) [55]:

$$B_x = \frac{B_r}{2}\cdot\left[\frac{T+x}{\sqrt{R^2+(T+x)^2}} - \frac{x}{\sqrt{R^2+x^2}}\right] \quad (1)$$

where T is the magnet thickness, and R is the magnet radius. The

Table 2
Energy dispersive X-ray spectrometer (EDS) Results.

Material	C		O		Fe		Co	
	Mass %	Atom %	Mass %	Atom %	Mass %	Atom %	Mass %	Atom %
PVA	58.34	65.11	41.66	34.89	–	–	–	–
$CoFe_2O_4$	–	–	30.68	61.20	42.39	24.22	26.93	14.58
PVA/1.25 % $CoFe_2O_4$	59.05	65.95	40.48	33.94	0.32	0.08	0.16	0.04
PVA/2.5 % $CoFe_2O_4$	57.73	66.34	37.74	32.56	3.01	0.74	1.52	0.36
PVA/5% $CoFe_2O_4$	56.46	65.49	38.10	33.17	3.49	0.87	1.95	0.46

actuation response was recorded using a high-speed camera (Sony RX100 IV), and the actuation distance (Δ) was measured using FIJI-ImageJ software.

2.5. Cell Culture and cytotoxicity analysis

Mouse Embryonic Fibroblasts (MEFs) were used to assess cytotoxicity release by PVA/$CoFe_2O_4$ MAPCs films. The cells were cultured in DMEM GlutaMAX™ (Gibco), supplemented with 10 % fetal bovine serum (FBS), 1 % antibiotic–antimycotic solution, and 1x non-essential amino acids. 5000 cells were seeded into 48-well plates and incubated at 37 °C with 5 % CO_2 and 20 % O_2 for 24 h. After the initial 24-hour incubation period, the media was replaced with media containing 25 × 25 mm PVA/$CoFe_2O_4$ MAPCs films. The 25x25 mm PVA/$CoFe_2O_4$ MAPCs films were incubated in 5 ml of media for a period of ≥ 5 days before being added to MEFs. After 72 h of incubation of the MEFs in media containing PVA/$CoFe_2O_4$ MAPCs films, cell viability was assessed using 0.2 % crystal violet assay, a commonly used method to access cytotoxicity [56]. The wells were washed with 1X PBS and treated with 0.2 % crystal violet for 30 min, followed by four five-minute 1X PBS washes. The plate was then left to air dry and imaged the following day using the iBright1500 imaging system (Invitrogen). Images were analysed with FIJI-ImageJ software. TIFF images were converted to threshold images. The regions of interest (ROI) manager was used to measure the intensity of the stain within the wells. Statistical analysis was performed on GraphPad Prism software, and the *P*-values were calculated using an unpaired *t*-test.

3. Results and Discussions

3.1. Scanning electron microscopy (SEM)

Scanning electron microscopy (SEM) was performed to investigate the morphology of the base materials (i.e., PVA and $CoFe_2O_4$) and MAPC (PVA/$CoFe_2O_4$) films. The SEM images of the MAPC films for different concentrations are reported in Fig. 3 under different magnification levels. The SEM images confirmed the increase in $CoFe_2O_4$ nanoparticles content in the respective MAPC films. $CoFe_2O_4$ nanoparticles were homogeneously dispersed within the PVA matrix, especially at lower concentrations; however, some agglomerations were observed at higher concentrations (i.e., 5 %). In addition, the energy-dispersive X-ray spectroscopy (EDS) analysis identified the elemental composition of the PVA, $CoFe_2O_4$, and their composites containing 1.25 %, 2.5 %, and 5 % of $CoFe_2O_4$ by weight.

Table 2 summarises the results, showing the weight percentage (mass %) and atomic percentage (atom %) of each element (C, O, Fe, and Co) present in all the materials. As expected, the pure PVA sample contained only carbon (C) and oxygen (O), while $CoFe_2O_4$ nanoparticles showed a significant presence of iron (Fe), cobalt (Co), and oxygen (O). The EDS analysis successfully verified the presence of $CoFe_2O_4$ in the PVA-based MAPCs, as the PVA/$CoFe_2O_4$ MAPCs (PVA/1.25 % $CoFe_2O_4$, PVA/2.5 % $CoFe_2O_4$, and PVA/5% $CoFe_2O_4$) exhibited the presence of all the elements identified in the pure materials (C, O, Fe, and Co).

The weight and atomic percentages of C and O were comparable to pure PVA, indicating that PVA was the major constituent in all the composite formulations. It is worth noting that increasing amounts of Fe and Co were observed with the increasing $CoFe_2O_4$ content in the composites. The 1.25 % composite showed minimal Fe and Co presence, while the 5 % composite had the highest percentage of these elements. EDS is a semi-quantitative technique, so the exact weight percentages do not perfectly match the actual $CoFe_2O_4$ loading. However, the observed trend confirms the successful integration of $CoFe_2O_4$ into the PVA matrix. In addition, the increasing weight and atomic percentages of Fe and Co with higher $CoFe_2O_4$ content directly correlate with the increased $CoFe_2O_4$ content in different MAPCs.

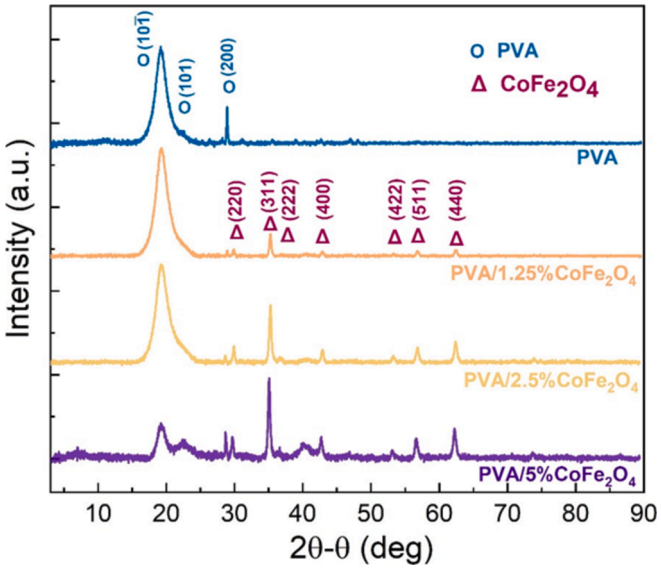

Fig. 4. X-Ray Diffraction (XRD)) results for synthesised magnetoactive polymer composite (MAPC) films at different $CoFe_2O_4$ nanoparticle concentrations within the PVA matrix.

3.2. X-ray diffraction (XRD)

Fig. 4 shows the XRD patterns for pure PVA and PVA/$CoFe_2O_4$ MAPCs with different $CoFe_2O_4$ concentrations. All samples possess diffraction peaks of PVA with the major peak (10$\bar{1}$) at $2\theta = 19.4^\circ$ being broad indicating poor crystallinity of PVA. However, the existence of this major peak implies that PVA chains tend to arrange themselves in a *trans*-planar conformation [57]. As the concentration of $CoFe_2O_4$ increases, XRD peaks attributed to $CoFe_2O_4$ become more visible where the maximum intensity is correlated with the maximum $CoFe_2O_4$ concentration. Multiple XRD peaks are observed for $CoFe_2O_4$ suggesting that its particles, with different crystallographic orientations, are homogeneously distributed in the PVA/$CoFe_2O_4$ MAPCs. It is worth noting the structure of PVA was persevered as $CoFe_2O_4$ concentration increased until 2.5 %. At 5 % of $CoFe_2O_4$, the intensity of PVA major peak (10$\bar{1}$) decreases tremendously, which could be attributed to the fact that PVA chain alignment is disturbed by the introduction of $CoFe_2O_4$ nanoparticles.

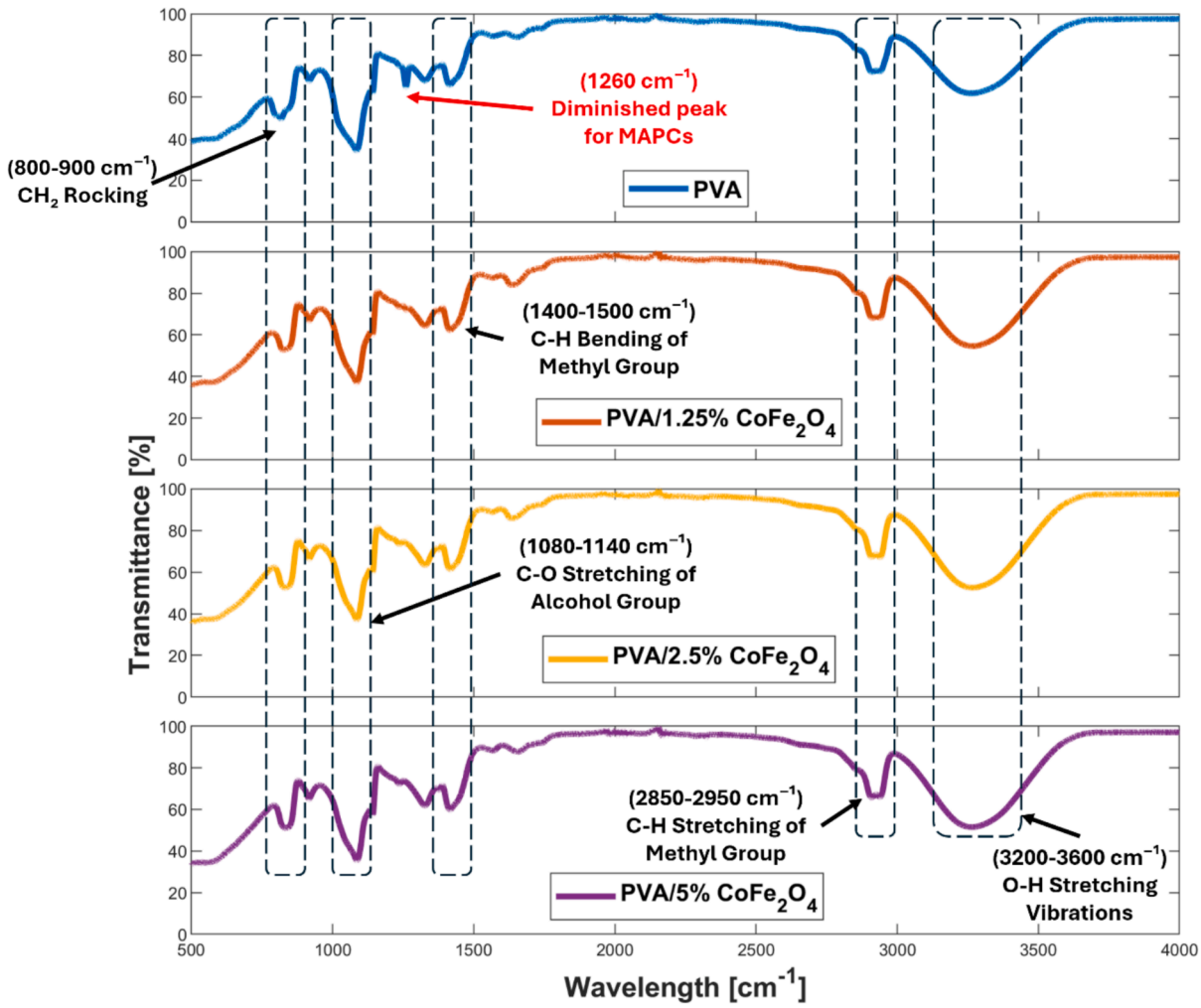

Fig. 5. Fourier transform infrared (FTIR) results for synthesised magnetoactive polymer composite (MAPC) films at different $CoFe_2O_4$ nanoparticle concentrations within the PVA matrix.

3.3. *Fourier transform infrared spectroscopy (FTIR)*

FTIR analysis was also performed to identify the chemical functional groups within the synthesised MACPs, as shown in Fig. 5. In the spectrum of neat PVA, characteristic peaks were observed at 3200–3600 cm^{-1}, 2850–2950 cm^{-1}, 1400–1500 cm^{-1}, 1080–1140 cm^{-1}, and 800–900 cm^{-1}, corresponding to the typical vibrational modes of the PVA polymer [58]. The broad peak at 3200–3600 cm^{-1} is attributed to the O–H stretching vibrations of the hydroxyl groups, which indicate the presence of hydrogen bonding. Peaks at 2850–2950 cm^{-1} are associated with the C–H stretching vibrations of the methylene (–CH_2–) groups in the polymer backbone. The C–H bending vibrations of the methylene groups were observed at 1400–1500 cm^{-1}, while the C–O stretching vibrations of the hydroxyl groups appeared in the region of 1080–1140 cm^{-1}. Finally, the rocking vibrations of the CH_2 groups were evident in the region of 800–900 cm^{-1}. These peaks are consistent with the typical FTIR spectrum of PVA, confirming the structural integrity of the polymer.

The addition of $CoFe_2O_4$ nanoparticles had a minimal effect on most of these characteristic peaks. The O–H stretching (3200–3600 cm^{-1}), C–H stretching (2850–2950 cm^{-1}), C–H bending (1400–1500 cm^{-1}), C–O stretching (1080–1140 cm^{-1}), and CH_2 rocking vibrations (800–900 cm^{-1}) remained relatively unchanged in terms of intensity and position, which indicates that the incorporation of $CoFe_2O_4$ nanoparticles did not significantly disrupt the structure of PVA or its primary functional groups. However, a notable change was observed at 1260 cm^{-1}, where a peak present in the neat PVA spectrum diminished significantly in the PVA/$CoFe_2O_4$ MAPCs. This peak is typically associated with the C–O stretching or C–O–H bending vibrations of the hydroxyl groups within the polymer matrix. The reduction in the intensity of this peak suggests an interaction between the hydroxyl groups of PVA and the surface of the $CoFe_2O_4$ nanoparticles. This interaction likely involves the formation of hydrogen bonds between the –OH groups in PVA and the metal oxide surface of the nanoparticles, or even a coordination interaction between the metal ions (Co or Fe) and the oxygen atoms in PVA. Such interactions may lead to a decrease in the free hydroxyl groups' vibrational freedom, which supports the diminished intensity of the peak at 1260 $cm^{-}1$.

Moreover, it is crucial to highlight the presence of specific vibrational modes associated with the Fe–O and Co–O bonds in the $CoFe_2O_4$ nanoparticles. In the spinel structure of $CoFe_2O_4$, Fe and Co ions occupy tetrahedral and octahedral sites [59]. Peaks corresponding to the stretching vibrations of the Fe–O bonds in the octahedral sites typically appear in the range of 400–600 cm^{-1}, while Co–O bonds, depending on their coordination, exhibit distinct vibrational modes that may overlap with other peaks in the spectrum [60]. However, these peaks are not evident in the FTIR results, probably due to lower $CoFe_2O_4$ nanoparticle concentrations. The unaffected other characteristic peaks indicate that the $CoFe_2O_4$ nanoparticles primarily interact with the hydroxyl groups, rather than causing widespread changes in the polymer's molecular structure. This localized interaction between PVA and $CoFe_2O_4$ nanoparticles has implications for the mechanical and magnetic properties of

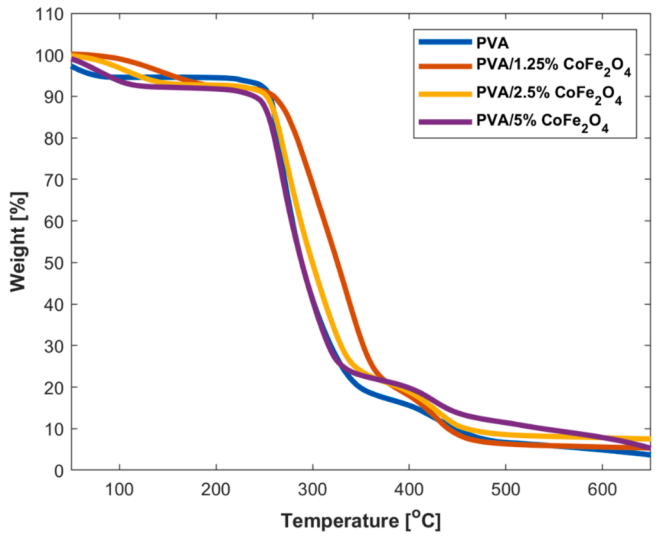

Fig. 6. Thermogravimetric analysis (TGA) results for synthesised magneto-active polymer composites (MAPCs). The initial weight loss in all the materials tested is attributed to the residual solvent evaporation. The first degradation at around 250-270℃ resulted in significant weight loss for all materials.

MAPCs, without significantly altering their chemical composition or backbone structure.

3.4. Thermogravimetric analysis (TGA)

Thermogravimetric analysis (TGA) was performed to observe the weight change with a temperature ramp of up to 650℃ in pure PVA and PVA/$CoFe_2O_4$ MAPCs, as reported in Fig. 6. All four materials exhibited a gradual weight loss as the temperature increased, indicating thermal decomposition. The initial weight loss at around 100℃ can be attributed to the evaporation of the residual solvent (water). A higher weight loss per cent in the PVA/$CoFe_2O_4$ MAPCs between 100 and 200℃ as compared to the pure PVA can be attributed to a higher residual solvent in composites. The onset of degradation occurred between around 250-270℃, resulting in significant weight loss for all materials. The pure PVA sample begins its significant weight loss around 260 °C, with a steep degradation slope occurring between 260 °C and 400 °C. However, an increased thermal stability for $CoFe_2O_4$ reinforced PVA composites was observed. The PVA/1.25 % $CoFe_2O_4$ MAPC exhibits the slowest rate of weight loss after the onset of degradation (around 270 °C). It retains more weight across the temperature range compared to pure PVA and higher-concentration MAPCs, indicating superior thermal stability. The enhanced thermal stability of the PVA/1.25 % $CoFe_2O_4$ MAPC may be attributed to the more uniform dispersion of $CoFe_2O_4$ nanoparticles at lower concentrations, which leads to stronger interfacial interactions between the polymer matrix and nanoparticles, which can hinder the mobility of polymer chains, thereby delaying thermal degradation. The PVA/2.5 % $CoFe_2O_4$ MAPC shows a slightly faster degradation compared to the PVA/1.25 % MAPC but still retains more weight over the degradation temperature than the pure PVA. The PVA/5% $CoFe_2O_4$ MAPC, while still more thermally stable than pure PVA, shows the highest weight loss among the MAPCs after degradation starts, with a rapid decomposition beginning at around 265 °C. At higher $CoFe_2O_4$ contents (2.5 % and 5 %), the onset of thermal degradation occurs at lower temperatures, likely due to particle agglomeration, which reduces the effective surface area for interaction with the matrix. The $CoFe_2O_4$ nanoparticles agglomeration may create localized stress points that accelerate thermal decomposition, leading to the observed decrease in thermal stability. The lower weight loss in the MAPCs compared to pure PVA confirms that $CoFe_2O_4$ nanoparticles enhance thermal stability [61]. $CoFe_2O_4$ likely acts as a barrier, hindering heat from diffusing within the PVA matrix and improving thermal stability. Finally, the residual weight per cent in all the materials is attributed to the $CoFe_2O_4$ nanoparticles having significantly higher decomposition temperatures and PVA decomposition residuals.

Table 3
Magnetic Properties of Base Materials (PVA and $CoFe_2O_4$) and Synthesised MAPCs.

Material	Saturation (M_s, EMU/g)	Coercivity (H_c, Oe)	Remanence (M_r, EMU/g)
PVA	–	–	–
$CoFe_2O_4$	52.56	2438	30.8
PVA/1.25 % $CoFe_2O_4$	0.345	2536	0.208
PVA/2.5 % $CoFe_2O_4$	0.640	2480	0.374
PVA/5% $CoFe_2O_4$	2.69	2411	1.59

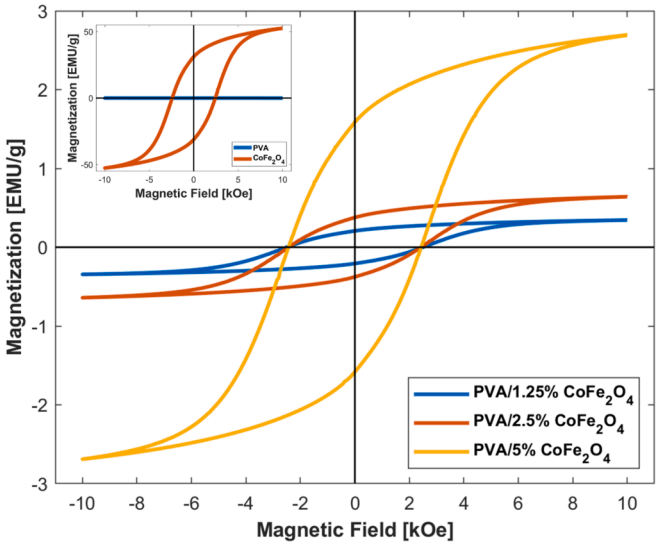

Fig. 7. Vibrating sample magnetometer (VSM) results for synthesised magneto-active polymer composites (MAPCs). The subplot presents the magnetisation profile of PVA and $CoFe_2O_4$ nanopowder, while the main plot represents the magnetisation profiles for the MAPCs. The resulting magnetisation of the MAPCs increases significantly with the increase in $CoFe_2O_4$ concentrations.

3.5. Magnetic properties (Vibrating sample Magnetometer)

Table 3 and Fig. 7 present the tabular and visual illustration of the magnetic properties of pure PVA, $CoFe_2O_4$, and the synthesised PVA/$CoFe_2O_4$ MAPCs with varying $CoFe_2O_4$ content (1.25 %, 2.5 %, and 5 %). Pure PVA, a nonmagnetic polymer, exhibited no measurable magnetic properties (as evident from the Fig. 7 subplot). $CoFe_2O_4$, the ferromagnetic component, demonstrated a high saturation magnetisation (52.56 EMU/g), which indicates that $CoFe_2O_4$ can be strongly magnetised when placed in an external magnetic field. A high saturation magnetisation also suggests a large number of moments within the material that can align with the applied magnetic field. Furthermore, $CoFe_2O_4$ exhibited a relatively high coercivity (2438 Oe), signifying resistance to any demagnetisation (i.e., once $CoFe_2O_4$ is magnetised, it can retain its magnetism even when the external magnetic field is removed). The remanence (30.8 EMU/g) of $CoFe_2O_4$ represents the residual magnetism that remains after the external field is withdrawn. The PVA/$CoFe_2O_4$ MAPCs exhibited a significant enhancement in magnetic properties with increasing $CoFe_2O_4$ content, as evident by the saturation magnetization (Ms), coercivity (Hc), and remanence (Mr). The magnetic

behaviour of $CoFe_2O_4$, a spinel ferrite, is highly dependent on the distribution of cations (Co^{2+} and Fe^{3+}) between tetrahedral (A) and octahedral (B) sites in the spinel structure [62]. Co^{2+} ions preferentially occupy the octahedral sites, while Fe^{3+} ions are distributed between tetrahedral and octahedral sites. This cation distribution governs the magnetic interactions within the material, particularly the superexchange interactions between Fe^{3+} ions at A and B sites, and Co^{2+} ions at B sites, which influence the magnetic properties observed in the MAPCs [63].

For the PVA/1.25 % $CoFe_2O_4$ MAPC, the hysteresis loop exhibited a significantly lower Ms = 0.345 EMU/g, Hc = 2536 Oe, and Mr = 0.208 EMU/g. The low Ms and Mr values indicate that the small amount of $CoFe_2O_4$ nanoparticles only weakly contribute to the overall magnetization of the MAPC. Despite the minimal magnetic response, the non-zero magnetic properties suggest a weak ferromagnetic behaviour due to the dispersed $CoFe_2O_4$ nanoparticles. At this concentration, the limited number of nanoparticles results in fewer available magnetic moments from the Co^{2+} and Fe^{3+} cations at octahedral and tetrahedral sites, respectively, which weakens the overall magnetic interaction. The slightly higher Hc value (2536 Oe) compared to pure $CoFe_2O_4$ may be attributed to the influence of the PVA matrix, which restricts the alignment of magnetic domains, resulting in higher resistance to magnetization reversal.

For the PVA/2.5 % $CoFe_2O_4$ MAPC, the magnetic properties revealed a notable improvement (Ms = 0.640 EMU/g, Hc = 2480 Oe, and Mr = 0.374 EMU/g). The increase in Ms and Mr values indicates that a higher concentration of $CoFe_2O_4$ nanoparticles leads to a more significant contribution to the overall magnetic behaviour, as more magnetic moments are available to align in an external magnetic field. As the concentration of $CoFe_2O_4$ increases, the higher number of Co^{2+} ions occupying octahedral sites and Fe^{3+} ions at both A and B sites enhances the magnetic interactions through superexchange, contributing to the increase in Ms and Mr. The slight decrease in Hc compared to the PVA/1.25 % $CoFe_2O_4$ composite suggests that with higher $CoFe_2O_4$ content, the closer nanoparticles allow easier domain wall movement and reduce the coercivity. Finally, PVA/5% $CoFe_2O_4$ MAPC exhibited the most substantial magnetic properties (Ms = 2.69 EMU/g, Hc = 2411 Oe, and Mr = 1.59 EMU/g). The significant increase in Ms and Mr with higher $CoFe_2O_4$ content indicates that more magnetic moments from the embedded nanoparticles can be aligned, resulting in stronger magnetization. At this concentration, the higher density of Co^{2+} and Fe^{3+} ions enhances the superexchange interactions, particularly between Fe^{3+} ions at A and B sites, leading to stronger magnetic coupling and higher overall magnetization. The slightly reduced Hc (2411 Oe) further evidences that at higher concentrations, the nanoparticles are more closely packed, which decreases domain wall pinning and makes magnetization reversal easier. Improvement in magnetic properties is consistent with the increasing $CoFe_2O_4$ content, where higher nanoparticle concentrations contribute more magnetic moments to the overall MAPC, leading to stronger magnetic responses. The tunability of these properties by varying the $CoFe_2O_4$ content opens doors for potential applications in areas like remote magnetic actuation and/or targeted drug delivery.

3.6. Magnetic actuation response

The magnetic actuation response was achieved by placing a permanent disc magnet at different distances from a MAPC sample with a varying magnetic flux density from 0 to 2900G. Pure PVA samples did not respond to the magnetic field, as they have nonmagnetic intrinsic properties, which is also evident from the magnetic properties characterised by VSM. $CoFe_2O_4$ incorporated PVA MAPCs responded to the applied magnetic fields at higher magnetic flux densities, and composite samples rapidly bent to touch the permanent magnet. A maximum deflection of the samples was observed to be 27 mm, 32 mm, and 40 mm for PVA/1.25 % $CoFe_2O_4$, PVA/2.5 % $CoFe_2O_4$, and PVA/5% $CoFe_2O_4$ at the maximum magnetic field intensities, respectively. All samples

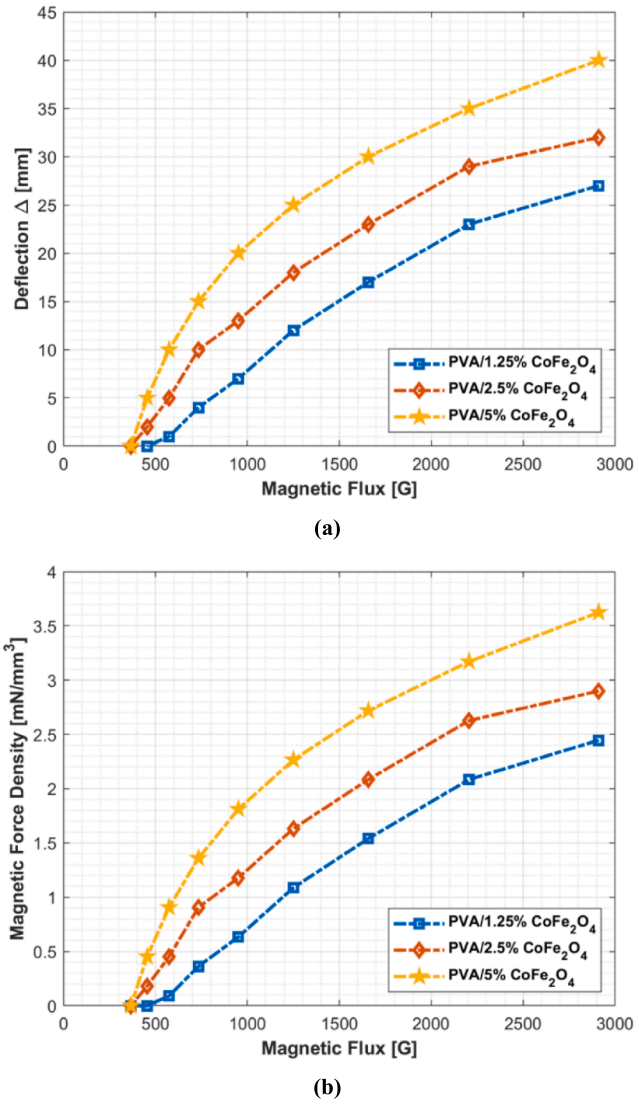

Fig. 8. Magnetic actuation results for different magnetoactive polymer composites (MAPCs). **(a)** Magnetic flux vs deflection represents the displacement of MAPC films with increased magnetic flux. An increased deflection of MAPC films was observed for higher magnetic flux and increased $CoFe_2O_4$ concentrations in PVA **(b)** Magnetic flux vs magnetic force density represents the magnetic force induced into the MAPC films per unit volume. An increased magnetic force density of MAPC films was observed for higher magnetic flux and increased $CoFe_2O_4$ concentrations in PVA.

recovered their initial shapes and forms after removing the magnetic field within a few seconds. Magnetic actuation of the MAPC samples is mainly due to the interaction between the applied magnetic field and the magnetic nanoparticles within the PVA polymer matrix [64]. A magnetic dipole moment is induced within the magnetic nanoparticles due to the presence of a magnetic field, and magnetic nanoparticles tend to align in the direction of the applied magnetic field, resulting in the deflection of MAPC samples [65–67]. The net force exerted on the MAPCs due to the applied magnetic field can be calculated using the following classical beam theory:

$$F_m = \frac{2EI\Delta}{(L_s)^3}$$

where Δ is the deflection, E is Young's modulus, and I is the second moment of inertia calculated from $t^3w/12$, where t – sample thickness and w – sample width. Fig. 8 reports the magnetic actuation response

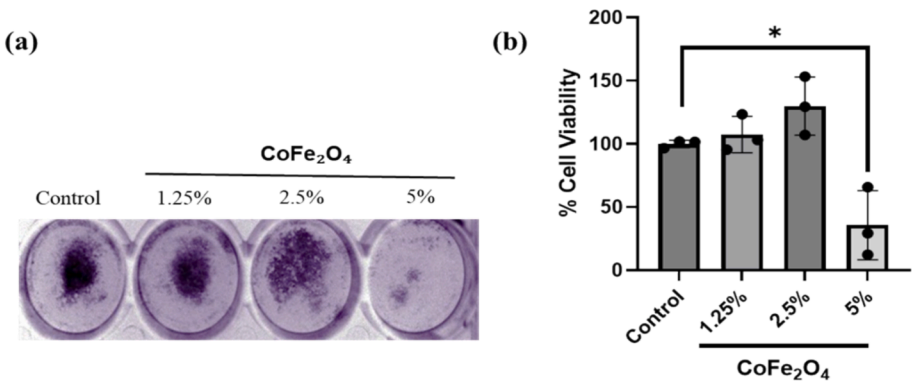

Fig. 9. Cytotoxicity analysis of the PVA/$CoFe_2O_4$ films on Mouse Embryonic Fibroblasts (MEFs) **(a)** Crystal violet cytotoxicity analysis of MEFs incubated in media with 25x25mm sheets of PVA/ $CoFe_2O_4$ films at 1.25 %, 2.5 % and 5 %; the control is DMEM media with no sheets incubated. **(b)** Quantification of the cytotoxicity analysis, showing the percentage of MEFs viable after 72 h of incubation in PVA/ $CoFe_2O_4$ film at 1.25 %, 2.5 % and 5 %. The data shown are three biological replicates analysed by unpaired t-tests with a 95 % confidence level. (*) P-value = 0.0155.

and applied force densities (F_m/V) on the PVA/$CoFe_2O_4$ MAPCs under different magnetic field intensities.

The magnetic actuation results show that the deflection and force densities increase with the increase in the magnetic flux density due to higher magnetic dipole moments, resulting in higher interactions [68]. A minimum magnetic flux density of 570G was required to activate the magnetic actuation for all the PVA/$CoFe_2O_4$ MAPC compositions. In addition, the sample deflections and induced force densities also increase with the increase in the $CoFe_2O_4$ nanoparticle concentrations for a specific magnetic flux density due to the stronger interaction of the magnetic field with the $CoFe_2O_4$ nanoparticles [69]. From magnetic actuation results, it is evident that such novel materials can potentially be used in applications requiring controlled response/displacement/ actuation under applied magnetic fields by fine-tuning the magnetic fields and magnetic particle concentrations within the polymer matrices [70,71].

3.7. Cytotoxicity release from PVA/$CoFe_2O_4$ films

$CoFe_2O_4$ has been reported to induce a cytotoxic effect on cells at high concentrations [72,73]. Investigating the film composition for any cytotoxic release for biomedical applications is crucial to ensure the material does not induce cell death. To evaluate potential cytotoxicity from different material combinations, 25x25 mm sheets of the PVA/ $CoFe_2O_4$ films at 1.25 %, 2.5 % and 5 % $CoFe_2O_4$ concentrations were incubated in 5 ml of media for a period of $\geq$ 5 days to release any components that could potentially induce a cytotoxic effect on cells. The media containing the released components was then used on Mouse Embryonic Fibroblasts (MEFs), and the cytotoxic effect was assessed after 72 h of incubation. Films with $CoFe_2O_4$ percentages of 1.25 % and 2.5 % showed no cytotoxic effect on the cells (Fig. 9 **(a) and (b))**. However, at 5 %, a significant toxic effect was observed, with an average of 35 % of the cells being viable (Fig. 9 **(a) and (b))**. This aligns with previous studies, which report that higher concentrations of $CoFe_2O_4$ induce cytotoxic effects [72,73].

4. Conclusions & future scope

In this work, novel MAPCs were synthesised comprising polyvinyl alcohol (PVA) as the polymer matrix and cobalt iron oxide ($CoFe_2O_4$) nanoparticles as the magnetic fillers with varying concentrations (i.e., 1.25 %, 2.5 %, and 5 %). PVA/$CoFe_2O_4$ MAPCs were synthesised using solution casting technique, and SEM analysis of MAPC films confirmed homogeneous dispersion of $CoFe_2O_4$ nanoparticles at lower concentrations, with some agglomeration at 5 %. EDS results verified the presence of Co, Fe, C, and O elements, showing increasing Fe and Co content with higher $CoFe_2O_4$ loading, indicating successful integration into the PVA matrix. XRD analysis showed that pure PVA exhibits a broad peak at $2\theta = 19.4^\circ$ indicating poor crystallinity. With increasing $CoFe_2O_4$ content, $CoFe_2O_4$ peaks became more prominent, and the major PVA peak's intensity decreased at 5 % $CoFe_2O_4$, suggesting disrupted PVA chain alignment due to $CoFe_2O_4$ nanoparticle incorporation. FTIR analysis showed characteristic PVA peaks remained mostly unchanged upon adding $CoFe_2O_4$ nanoparticles, indicating preserved polymer structure. However, a significant reduction at 1260 cm^{-1} suggested interactions between PVA hydroxyl groups and $CoFe_2O_4$, possibly via hydrogen bonding or coordination with metal ions. Thermogravimetric analysis revealed that $CoFe_2O_4$-reinforced PVA MAPCs exhibit enhanced thermal stability compared to pure PVA, with the 1.25 % $CoFe_2O_4$ MAPC showing the highest stability due to uniform nanoparticle dispersion. Higher $CoFe_2O_4$ content led to reduced stability due to nanoparticle agglomeration. The magnetic properties of PVA/$CoFe_2O_4$ MAPCs increase with higher $CoFe_2O_4$ content, as shown by rising saturation magnetization (Ms), remanence (Mr), and a decrease in coercivity (Hc). The improvement in Ms and Mr is attributed to increased superexchange interactions between $Fe3^+$ and $Co2^+$ ions at tetrahedral and octahedral sites, whereas the slight reduction in Hc is due to easier domain wall movement with higher $CoFe_2O_4$ nanoparticle density. Magnetic actuation of PVA/$CoFe_2O_4$ MAPCs showed increasing deflection (up to 40 mm) and force density with higher magnetic flux densities (0-2900G) and $CoFe_2O_4$ content. The actuation, starting at 570G, results from magnetic dipole moments induced in the nanoparticles, with stronger magnetic interactions at higher nanoparticle concentrations enhancing the response. Cytotoxicity testing of PVA/$CoFe_2O_4$ films showed no adverse effects on Mouse Embryonic Fibroblasts at 1.25 % and 2.5 % $CoFe_2O_4$, while a 5 % concentration significantly reduced cell viability to 35 %, confirming higher $CoFe_2O_4$ levels can induce cytotoxic effects.

In subsequent research, more comprehensive biological testing will be performed to explore different additives to PVA/$CoFe_2O_4$ MAPCs to improve their biological performances (regarding biocompatibility, cell adhesion and cytocompatibility). In future studies, synthesised MAPCs will also be converted into feedstock materials (i.e., filaments, inks) for additive manufacturing processes (i.e., fused filament fabrication and direct ink writing). Novel design ideas can be prototyped and tested owing to the flexibility in designing and fabrication using these additive manufacturing processes. Integrating advanced manufacturing processes for smart materials will further open new avenues for such novel materials in remote actuation and sensing for broader applications, specifically biomedical engineering [74].

CRediT authorship contribution statement

Ans Al Rashid: Writing – review & editing, Writing – original draft, Visualization, Validation, Methodology, Investigation, Formal analysis, Data curation, Conceptualization. **Noor A. Al-Maslamani:** Writing – original draft, Visualization, Validation, Investigation, Formal analysis, Data curation. **Anas Abutaha:** Writing – original draft, Formal analysis, Data curation. **Mokarram Hossain:** Writing – review & editing, Supervision. **Muammer Koç:** Writing – review & editing, Supervision, Resources, Project administration, Funding acquisition.

Declaration of competing interest

The authors declare that they have no known competing financial interests or personal relationships that could have appeared to influence the work reported in this paper.

Acknowledgements

The authors would like to acknowledge Qatar National Research Fund (QNRF) for its support through the grant (NPRP13S-0126-200172) and HBKU Innovation Center for its support through Industrial Innovation Fund (HBKU-OIIR-IIF-07-01) that made this work possible partially. Open Access funding provided by the Qatar National Library (QNL). The authors would also like to acknowledge the HBKU core labs for their support in characterising the samples. M. H. acknowledges the support of the Royal Society (UK) through the International Exchange Grant (IEC/NFSC/211316).

Data availability

Data will be made available on request.

References

[1] S. Lucarini, M. Hossain, D. Garcia-Gonzalez, Recent advances in hard-magnetic soft composites: Synthesis, characterisation, computational modelling, and applications, Compos. Struct 279 (2022), https://doi.org/10.1016/j.compstruct.2021.114800.

[2] H. Liu, F. Wang, W. Wu, X. Dong, L. Sang, 4D printing of mechanically robust PLA/TPU/Fe3O4 magneto-responsive shape memory polymers for smart structures, Compos. B. Eng 248 (2023) 110382, https://doi.org/10.1016/j.compositesb.2022.110382.

[3] D. Garcia-Gonzalez, M.A. Moreno, L. Valencia, A. Arias, D. Velasco, Influence of elastomeric matrix and particle volume fraction on the mechanical response of magneto-active polymers, Compos. B. Eng 215 (2021) 108796, https://doi.org/10.1016/j.compositesb.2021.108796.

[4] O.V. Stolbov, Y.L. Raikher, Magnetostrictive and Magnetoactive Effects in Piezoelectric Polymer Composites, Nanomaterials 14 (2024), https://doi.org/10.3390/nano14010031.

[5] G.V. Stepanov, A.V. Bakhtiiarov, D.A. Lobanov, P.A. Storozhenko, Magnetoresistivity and piezoresistivity of magnetoactive elastomers, J. Magn. Magn. Mater 587 (2023) 171313, https://doi.org/10.1016/j.jmmm.2023.171313.

[6] A.K. Bastola, M. Paudel, L. Li, W. Li, Recent progress of magnetorheological elastomers: a review, Smart. Mater. Struct 29 (2020) 123002, https://doi.org/10.1088/1361-665X/abbc77.

[7] J.A. Silva, C. Gouveia, G. Dinis, A.M. Pinto, A.M. Pereira, Giant magnetostriction in low-concentration magnetorheological elastomers, Compos. B. Eng 243 (2022) 110125, https://doi.org/10.1016/j.compositesb.2022.110125.

[8] M.A. Moreno-Mateos, M. Hossain, P. Steinmann, D. Garcia-Gonzalez, Hybrid magnetorheological elastomers enable versatile soft actuators, NPJ. Comput. Mater 8 (2022) 162, https://doi.org/10.1038/s41524-022-00844-1.

[9] Y. Shou, L. Liu, Q. Liu, Z. Le, K.L. Lee, H. Li, X. Li, D.Z. Koh, Y. Wang, T.M. Liu, Z. Yang, C.T. Lim, C. Cheung, A. Tay, Mechano-responsive hydrogel for direct stem cell manufacturing to therapy, Bioact. Mater 24 (2023) 387–400, https://doi.org/10.1016/j.bioactmat.2022.12.019.

[10] G. Cedillo-Servin, O. Dahri, J. Meneses, J. van Duijn, H. Moon, F. Sage, J. Silva, A. Pereira, F.D. Magalhães, J. Malda, N. Geijsen, A.M. Pinto, M. Castilho, 3D Printed magneto-active microfiber scaffolds for remote stimulation and guided organization of 3D in vitro skeletal muscle models, Small 20 (2024) 2307178, https://doi.org/10.1002/smll.202307178.

[11] A. Roy, Z. Zhang, M.K. Eiken, A. Shi, A. Pena-Francesch, C. Loebel, Programmable tissue folding patterns in structured hydrogels, Adv. Mater. n/a (n.d.) 2300017. doi: 10.1002/adma.202300017.

[12] A.K. Bastola, M. Hossain, The shape – morphing performance of magnetoactive soft materials, Mater. Des 211 (2021) 110172, https://doi.org/10.1016/j.matdes.2021.110172.

[13] S.K. Behera, D. Kumar, C.S. Maurya, S. Sarangi, Universal rate-dependence in electro-magneto-active polymeric composites, Compos. Sci. Technol 237 (2023) 110015, https://doi.org/10.1016/j.compscitech.2023.110015.

[14] S.A. Moezi, R. Sedaghati, S. Rakheja, Development of a novel nonlinear model and control strategy for soft continuum robots featuring hard magnetoactive elastomers, Smart. Mater. Struct 33 (2024) 45025, https://doi.org/10.1088/1361-665X/ad31d0.

[15] J. Xue, Z. Tian, X. Xiao, C. Du, S. Niu, Z. Han, Y. Liu, Magnetoactive soft materials with programmable magnetic domains for multifunctional actuators, ACS Appl. Mater. Interfaces 15 (2023) 56223–56232, https://doi.org/10.1021/acsami.3c11842.

[16] M. Wajahat, J.H. Kim, J.H. Kim, I.D. Jung, J. Pyo, S.K. Seol, 4D Printing of ultrastretchable magnetoactive soft material architectures for soft actuators, ACS. Appl. Mater. Interfaces 15 (2023) 59582–59591, https://doi.org/10.1021/acsami.3c12173.

[17] Z. Liao, O. Zoumhani, C.M. Boutry, Recent advances in magnetic polymer composites for BioMEMS: a review, Materials 16 (2023), https://doi.org/10.3390/ma16103802.

[18] Y. Kim, X. Zhao, Magnetic Soft Materials and Robots, Chem. Rev 122 (2022) 5317–5364, https://doi.org/10.1021/acs.chemrev.1c00481.

[19] E. Rossegger, R. Höller, K. Hrbinič, M. Sangermano, T. Griesser, S. Schlögl, 3D Printing of Soft Magnetoactive Devices with Thiol-Click Photopolymer Composites, Adv. Eng. Mater 25 (2023) 2200749, https://doi.org/10.1002/adem.202200749.

[20] J. Zhang, H. Pang, Y. Wang, X. Gong, The magneto-mechanical properties of off-axis anisotropic magnetorheological elastomers, Compos. Sci. Technol 191 (2020), https://doi.org/10.1016/j.compscitech.2020.108079.

[21] F.J. Vazquez-Perez, C. Gila-Vilchez, J.D.G. Duran, A. Zubarev, L. Alvarez de Cienfuegos, L. Rodriguez-Arco, M.T. Lopez-Lopez, Composite polymer hydrogels with high and reversible elongation under magnetic stimuli, Polymer (guildf) 230 (2021), https://doi.org/10.1016/j.polymer.2021.124093.

[22] D. Garcia-Gonzalez, T. Ter-Yesayants, M.A. Moreno-Mateos, M.L. Lopez-Donaire, Hard-magnetic phenomena enable autonomous self-healing elastomers, Compos. B. Eng 248 (2023), https://doi.org/10.1016/j.compositesb.2022.110357.

[23] D. Takahashi, A.V.S. Sainath, J. Ikeda, K. Budpud, T. Kaneko, M. Kawai, T. Mitsumata, Magnetorheological response for magnetic elastomers containing carbonyl iron particles coated with poly(Methyl methacrylate), Polymers. (basel) 13 (2021) 1–9, https://doi.org/10.3390/polym13030335.

[24] S. Jang, S. Park, 4D printed untethered milli-gripper fabricated using a biodegradable and biocompatible electro- and magneto-active hydrogel, Sens. Actuators. B. Chem 384 (2023) 133654, https://doi.org/10.1016/j.snb.2023.133654.

[25] M.S. Islam, T.G. Molley, T. Hung, C.I. Sathish, V.D.L. Putra, G.K. Jalandhra, J. Ireland, Y. Li, J. Yi, J.J. Kruzic, K.A. Kilian, Magnetic Nanofibrous Hydrogels for Dynamic Control of Stem Cell Differentiation, ACS Appl. Mater. Interfaces 15 (2023) 50663–50678, https://doi.org/10.1021/acsami.3c07021.

[26] J.C. Breger, C. Yoon, R. Xiao, H.R. Kwag, M.O. Wang, J.P. Fisher, T.D. Nguyen, D. H. Gracias, Self-folding thermo-magnetically responsive soft microgrippers, ACS Appl. Mater. Interfaces 7 (2015) 3398–3405, https://doi.org/10.1021/am508621s.

[27] M. Vasilyeva, D. Nagornov, G. Orlov, Research on dynamic and mechanical properties of magnetoactive elastomers with high permeability magnetic filling agent at complex magneto-temperature exposure, Materials 14 (2021), https://doi.org/10.3390/ma14092376.

[28] K. Chen, K. Nagashima, S. Takahashi, T. Komatsuzaki, M. Kawai, T. Mitsumata, Magnetically tunable transmissibility for magneto-responsive elastomers consisting of magnetic and nonmagnetic particles, ACS Appl. Polym. Mater 4 (2022) 2917–2924, https://doi.org/10.1021/acsapm.2c00181.

[29] D. Borin, G. Stepanov, A. Musikhin, A. Zubarev, A. Bakhtiiarov, P. Storozhenko, Magnetorheological effect of magnetoactive elastomer with a permalloy filler, Polymers (basel) 12 (2020) 1–25, https://doi.org/10.3390/polym12102371.

[30] V.G. Kolesnikova, L.A. Makarova, A.S. Omelyanchik, K.V. Sobolev, D.A. Isaev, I. A. Alekhina, A.S. Komlev, V.V. Rodionova, N.S. Perov, Magnetoactive elastomers based on ferromagnetic and ferroelectric particles: A FORC approach, J. Magn. Magn. Mater 558 (2022), https://doi.org/10.1016/j.jmmm.2022.169506.

[31] A. Bastola, M. Hossain, Enhanced performance of core-shell hybrid magnetorheological elastomer with nanofillers, Mater. Lett 297 (2021), https://doi.org/10.1016/j.matlet.2021.129944.

[32] A.K. Bastola, E. Ang, M. Paudel, L. Li, Soft hybrid magnetorheological elastomer: Gap bridging between MR fluid and MR elastomer, Colloids. Surf. A. Physicochem. Eng. Asp 583 (2019), https://doi.org/10.1016/j.colsurfa.2019.123975.

[33] G.W. Kim, S.W. Hong, J.Y. Yoon, S.K. Lee, S.H. Kim, S.B. Choi, A new magnetic-responsive hybrid soft composite with tunable equivalent tensile modulus: A proof-of-concept, Smart. Mater. Struct 29 (2020), https://doi.org/10.1088/1361-665X/ab8750.

[34] A.K. Bastola, V.T. Hoang, L. Li, A novel hybrid magnetorheological elastomer developed by 3D printing, Mater. Des 114 (2017) 391–397, https://doi.org/10.1016/j.matdes.2016.11.006.

[35] C. Kadapa, M. Hossain, A unified numerical approach for soft to hard magneto-viscoelastically coupled polymers, Mech. Mater. 166 (2022) 104207, https://doi.org/10.1016/j.mechmat.2021.104207.

[36] F. Dadgar-Rad, M. Hossain, A micropolar shell model for hard-magnetic soft materials, Int. J. Numer. Methods. Eng 124 (2023) 1798–1817, https://doi.org/10.1002/nme.7188.

[37] F. Dadgar-Rad, M. Hossain, Finite deformation analysis of hard-magnetic soft materials based on micropolar continuum theory, Int. J. Solids. Struct 251 (2022) 111747, https://doi.org/10.1016/j.ijsolstr.2022.111747.
[38] L. Xia, Z. Hu, L. Sun, Multiscale numerical modeling of magneto-hyperelasticity of magnetorheological elastomeric composites, Compos. Sci. Technol 224 (2022) 109443, https://doi.org/10.1016/j.compscitech.2022.109443.
[39] D. Romeis, M. Saphiannikova, Effective magnetic susceptibility in magnetoactive composites, J. Magn. Magn. Mater 565 (2023), https://doi.org/10.1016/j.jmmm.2022.170197.
[40] E. Yarali, M. Baniasadi, A. Zolfagharian, M. Chavoshi, F. Arefi, M. Hossain, A. Bastola, M. Ansari, A. Foyouzat, A. Dabbagh, M. Ebrahimi, M.J. Mirzaali, M. Bodaghi, Magneto-/ electro-responsive polymers toward manufacturing, characterization, and biomedical/ soft robotic applications, Appl. Mater. Today 26 (2022) 101306, https://doi.org/10.1016/j.apmt.2021.101306.
[41] M. Wang, J. Bai, K. Shao, W. Tang, X. Zhao, D. Lin, S. Huang, C. Chen, Z. Ding, J. Ye, Poly(vinyl alcohol) Hydrogels: The Old and New Functional Materials, Int. J. Polym. Sci 2021 (2021) 2225426, https://doi.org/10.1155/2021/2225426.
[42] E. Malka, S. Margel, Engineering of PVA/PVP Hydrogels for Agricultural Applications, Gels 9 (2023), https://doi.org/10.3390/gels9110895.
[43] R. Abedi-Firoozjah, N. Chabook, O. Rostami, M. Heydari, A. Kolahdouz-Nasiri, F. Javanmardi, K. Abdolmaleki, A. Mousavi Khaneghah, PVA/starch films: An updated review of their preparation, characterization, and diverse applications in the food industry, Polym. Test. 118 (2023) 107903, https://doi.org/10.1016/j.polymertesting.2022.107903.
[44] E.A. Kamoun, S.A. Loutfy, Y. Hussein, E.-R.-S. Kenawy, Recent advances in PVA-polysaccharide based hydrogels and electrospun nanofibers in biomedical applications: A review, Int. J. Biol. Macromol 187 (2021) 755–768, https://doi.org/10.1016/j.ijbiomac.2021.08.002.
[45] Z. Karimzadeh, M. Mahmoudpour, E. Rahimpour, A. Jouyban, Nanomaterial based PVA nanocomposite hydrogels for biomedical sensing: Advances toward designing the ideal flexible/wearable nanoprobes, Adv. Colloid. Interface. Sci 305 (2022) 102705, https://doi.org/10.1016/j.cis.2022.102705.
[46] F. Ameen, N. Majrashi, Recent trends in the use of cobalt ferrite nanoparticles as an antimicrobial agent for disability infections: A review, Inorg. Chem. Commun 156 (2023) 111187, https://doi.org/10.1016/j.inoche.2023.111187.
[47] R. Ghorbanpour Ghartavool, G.R. Gordani, M.R. Loghman Estarki, M. Tavoosi, M. Mazaheri Forushani, E. Kiani, Synthesis, microstructure, magnetic and electromagnetic behavior of graphene oxide/hexagonal barium ferrite aerogel nanocomposites within the frequency range of 1–18 GHz, Arab. J. Chem. 16 (2023) 105099, https://doi.org/10.1016/j.arabjc.2023.105099.
[48] G.R. Gordani, M.R. Loghman Estarki, M. Danesh, E. Kiani, M. Tavoosi, Microstructure, phase, magnetic properties, and electromagnetic wave absorption of graphene oxide – Ni0.7Zn0.3Fe2O4 – Al2O3 aerogel, Ceram. Int 48 (2022) 3059–3069, https://doi.org/10.1016/j.ceramint.2021.10.081.
[49] T. Nypelö, C. Rodriguez-Abreu, J. Rivas, M.D. Dickey, O.J. Rojas, Magneto-responsive hybrid materials based on cellulose nanocrystals, Cellulose 21 (2014) 2557–2566, https://doi.org/10.1007/s10570-014-0307-2.
[50] M. Abu-Abdeen, O. Saber, E. Mousa, Preparation and physical characterization of cobalt iron oxide magnetic nanoparticles loaded polyvinyl alcohol, J. Thermoplastic Compos. Mater. 36 (2023) 201–217, https://doi.org/10.1177/0892705720985577.
[51] F. Ali, A. Al Rashid, S.N. Kalva, M. Koç, Mg-Doped PLA composite as a potential material for tissue engineering—synthesis, characterization, and additive manufacturing, Materials 16 (2023), https://doi.org/10.3390/ma16196506.
[52] F. Ali, S.N. Kalva, K.H. Mroue, K.S. Keyan, Y. Tong, O.M. Khan, M. Koç, Degradation assessment of Mg-Incorporated 3D printed PLA scaffolds for biomedical applications, Bioprinting 35 (2023) e00302.
[53] G.J.M. Antony, B.K. Bhavya, S. Raja, S.T. Aruna, Solvent casting-assisted synthesis of thermally responsive shape memory polymer and its composites, Polym. Bull. 80 (2023) 12211–12232, https://doi.org/10.1007/s00289-022-04651-y.
[54] A.K. Maurya, F.M. de Souza, T. Dawsey, R.K. Gupta, Biodegradable polymers and composites: Recent development and challenges, Polym. Compos 45 (2024) 2896–2918, https://doi.org/10.1002/pc.28023.
[55] K. Petcharoen, A. Sirivat, Magneto-electro-responsive material based on magnetite nanoparticles/polyurethane composites, Mater. Sci. Eng.:. C 61 (2016) 312–323, https://doi.org/10.1016/j.msec.2015.12.014.
[56] M. Feoktistova, P. Geserick, M. Leverkus, Crystal violet assay for determining viability of cultured cells, Cold. Spring. Harb. Protoc 2016 (2016) pdb-prot087379.
[57] R. Ricciardi, F. Auriemma, C. De Rosa, F. Lauprêtre, X-ray Diffraction Analysis of Poly(vinyl alcohol) Hydrogels, Obtained by Freezing and Thawing Techniques, Macromolecules 37 (2004) 1921–1927, https://doi.org/10.1021/ma035663q.
[58] J. Wang, L. Ye, Structure and properties of polyvinyl alcohol/polyurethane blends, Compos. B. Eng 69 (2015) 389–396, https://doi.org/10.1016/j.compositesb.2014.10.013.
[59] M.R. Loghman-Estarki, S. Torkian, R.A. Rastabi, A. Ghasemi, Effect of annealing temperature and copper mole ratio on the morphology, structure and magnetic properties of Mg0.5−xCuxZn0.5Fe2O4 nanoparticles prepared by the modified Pechini method, J. Magn. Magn. Mater. 442 (2017) 163–175, https://doi.org/10.1016/j.jmmm.2017.06.104.
[60] A. Ghasemi, M.R. Loghman-Estarki, S. Torkian, M. Tavoosi, The microstructure and magnetic behavior of spark plasma sintered iron/nickel zinc ferrite nanocomposite synthesized by the complex sol-gel method, Compos. B. Eng 175 (2019) 107179, https://doi.org/10.1016/j.compositesb.2019.107179.
[61] G.S.A. Suleiman, X. Zeng, R. Chakma, I.Y. Wakai, Y. Feng, Recent advances and challenges in thermal stability of PVA-based film: A review, Polym. Adv. Technol 35 (2024) e6327.
[62] K.L. Routray, S. Saha, Graphene nanoplatelets anchored into Ag doped spinel CoFe2O4 nanohybrid: Synthesis, structural, electrical, superior dielectric and room temperature induced ferromagnetism performance for high frequency device application, Diam. Relat. Mater 141 (2024) 110680, https://doi.org/10.1016/j.diamond.2023.110680.
[63] K.L. Routray, S. Saha, D. Behera, Insight Into the Anomalous Electrical Behavior, Dielectric and Magnetic Study of Ag-Doped CoFe2O4 Synthesised by Okra Extract-Assisted Green Synthesis, J. Electron. Mater 49 (2020) 7244–7258, https://doi.org/10.1007/s11664-020-08468-1.
[64] M. Zrinyi, 5 - Magnetically responsive polymer gels and elastomers: properties, synthesis and applications, in: M.R. Aguilar, J. San Román (Eds.), Smart Polymers and Their Applications, Woodhead Publishing, 2014, pp. 134–165, https://doi.org/10.1533/9780857097026.1.134.
[65] S. Ganguly, S. Margel, Review: Remotely controlled magneto-regulation of therapeutics from magnetoelastic gel matrices, Biotechnol. Adv 44 (2020) 107611, https://doi.org/10.1016/j.biotechadv.2020.107611.
[66] X. Guan, X. Dong, J. Ou, Magnetostrictive effect of magnetorheological elastomer, J. Magn. Magn. Mater 320 (2008) 158–163, https://doi.org/10.1016/j.jmmm.2007.05.043.
[67] J.G. Puente-Córdova, M.E. Reyes-Melo, B. López-Walle, I.Y. Miranda-Valdez, A. Torres-Castro, Characterization of a magnetic hybrid film fabricated by the in-situ synthesis of iron oxide nanoparticles into ethyl cellulose polymer, Cellulose 29 (2022) 3845–3857, https://doi.org/10.1007/s10570-022-04528-3.
[68] Z. Varga, G. Filipcsei, A. Szilágyi, M. Zrínyi, Electric and Magnetic Field-Structured Smart Composites, Macromol. Symp 227 (2005) 123–134, https://doi.org/10.1002/masy.200550912.
[69] N. Thummarungsan, A. Sirivat, Magneto-Responsive Biopolymer Composite Based on Plasticized Poly(Butylene Succinate-Co-Butylene Adipate) and Fe3O4 for Flexible Actuator Application, J. Polym. Environ (2024), https://doi.org/10.1007/s10924-024-03190-z.
[70] V.M. Macedo, N. Pereira, C.R. Tubio, P. Martins, C.M. Costa, S. Lanceros-Mendez, Carrageenan based printable magnetic nanocomposites for actuator applications, Compos. Sci. Technol 224 (2022) 109485, https://doi.org/10.1016/j.compscitech.2022.109485.
[71] X. Wang, B. Han, R.-P. Yu, F.-C. Li, Z.-Y. Zhao, Q.-C. Zhang, T.J. Lu, Magnetic-responsive Fe3O4 nanoparticle-impregnated cellulose paper actuators, Extreme. Mech. Lett 25 (2018) 53–59, https://doi.org/10.1016/j.eml.2018.10.003.
[72] M. Ahamed, M.J. Akhtar, M.A.M. Khan, H.A. Alhadlaq, A. Alshamsan, Cobalt iron oxide nanoparticles induce cytotoxicity and regulate the apoptotic genes through ROS in human liver cells (HepG2), Colloids. Surf. B. Biointerfaces 148 (2016) 665–673, https://doi.org/10.1016/j.colsurfb.2016.09.047.
[73] M.S. Khan, S.A. Buzdar, R. Hussain, A. Alouffi, M.T. Aleem, M. Farhab, M.A. Javid, R.W. Akhtar, I. Khan, M.M. Almutairi, Cobalt Iron Oxide (CoFe2O4) Nanoparticles Induced Toxicity in Rabbits, Vet. Sci 10 (2023), https://doi.org/10.3390/vetsci10080514.
[74] B.R. Rodriguez-Vargas, G. Stornelli, P. Folgarait, M.R. Ridolfi, A.F. Miranda Pérez, A. Di Schino, Recent advances in additive manufacturing of soft magnetic materials: a review, Materials 16 (2023), https://doi.org/10.3390/ma16165610.